Received: 4 March 2019 | Revised: 17 December 2019 | Accepted: 8 January 2020

DOI: 10.1002/cnm.3312

WILEY

SPECIAL ISSUE PAPER

Impact of tapering of arterial vessels on blood pressure, pulse wave velocity, and wave intensity analysis using one-dimensional computational model

Shima Abdullateef[1] | **Jorge Mariscal-Harana**[2] | **Ashraf W. Khir**[1]

[1]Department of Mechanical and Aerospace Engineering, Brunel University London, London, UK

[2]School of Biomedical Engineering and Imaging Sciences, King's College London, London, UK

Correspondence
Ashraf W. Khir, Brunel University London, Kingston Lane, Uxbridge, Middlesex, UB8 3PH, London, UK.
Email: ashraf.khir@brunel.ac.uk

Abstract

The angle of arterial tapering increases with ageing, and the geometrical changes of the aorta may cause an increase in central arterial pressure and stiffness. The impact of tapering has been primarily studied using frequency-domain transmission line theories. In this work, we revisit the problem of tapering and investigate its effect on blood pressure and pulse wave velocity (PWV) using a time-domain analysis with a 1D computational model. First, tapering is modelled as a stepwise reduction in diameter and compared with results from a continuously tapered segment. Next, we studied wave reflections in a combination of stepwise diameter reduction of straight vessels and bifurcations, then repeated the experiments with decreasing the length to physiological values. As the model's segments became shorter in length, wave reflections and re-reflections resulted in waves overlapping in time. We extended our work by examining the effect of increasing the tapering angle on blood pressure and wave intensity in physiological models: a model of the thoracic aorta and a model of upper thoracic and descending aorta connected to the iliac bifurcation. Vessels tapering inherently changed the ratio between the inlet and outlet cross-sectional areas, increasing the vessel resistance and reducing the compliance compared with non-tapered vessels. These variables influence peak and pulse pressure. In addition, it is well established that pulse wave velocity increases in an ageing arterial tree. This work provides confirmation that tapering induces reflections and offers an additional explanation to the observation of increased peak pressure and decreased diastolic pressure distally in the arterial tree.

KEYWORDS

arterial tapering, pulse wave velocity, 1D computational model, time-domain analysis, ageing

1 | INTRODUCTION

Age-related alteration in the arterial tree is associated with progression of cardiovascular disease.[1,2] It profoundly affects proximal aortic geometry compared with the distal parts of the arterial tree.[3,4] Aortic unfolding is a common clinical expression referring to the elongation and enlarging of the aortic arch diameter, and previous works proved that it increases the central arterial blood pressure and the arterial stiffness.[2,5-7]

One of the known normal characteristics of the arterial system is its tapered structure, that is, the area of an artery decreases gradually towards its outlet.[8] Analysing the dynamics of blood flow in tapered structures is vital for understanding the development of pressure. Furthermore, according to the findings of Hickson et al[9] and Charlton et al,[10] with ageing, the diameter at the level of the ascending aorta and the aortic arch increases while the diameter of descending aorta remains the same. This means an increased tapering angle with ageing and hence our interest in the effect of tapering and its variation.

Any discontinuity in the geometry or the elasticity of the arterial system generates reflections. Because of the spatially varying elastic properties of the vessels and the branching structure of the arterial tree, wave reflections are always present in vessels. These reflected waves can also be re-reflected multiple times,[11,12] causing intricate patterns in the pressure waveform. Although the identification of reflection site has been the focus of many studies, the detailed understanding of this matter is still not completely comprehensive.[13]

While the changes in capillary blood vessels can be well captured with Windkessel (Wk) models[14,15] and the impact of bifurcations has been previously studied,[16-19] the direct influence of tapering and its contribution to the reflections is not well documented and requires further investigation.

The earliest research considering the changes of cross-sectional area and its mechanical effects was probably conducted by Patel et al,[20] where the dimensions of various sites along the aorta were measured in 30 living dogs. However, the rate of tapering varies from species to species, and the ratio presented by Patel et al may not justify the tapering rate in humans. Later, other studies approached the problem using the concept of admittance in the cardiovascular system.[21,22] The drawback of this approach is the inability to study the axial location of the reflections. The basic assumption with this approach is that if the reduction in the cross-sectional area is sufficiently gradual and occurs over a considerably longer length compared with the wavelength, the reflected energy caused by the tapering is small and can be neglected as the wave travels through the vessel.

Regarding the alteration in pressure (P), Fung[23] suggested that if the energy transmits completely while the cross-sectional area is decreasing gradually, the amplitude of the pressure is proportional to the square root of the characteristic impedance (Z):

$$P = \text{constant} \times \sqrt{Z},\ Z = \frac{\rho c}{A}, \tag{1}$$

where ρ denotes blood density, A is the cross-sectional area of the vessel, and c is the pulse wave velocity. With a reduction in the cross-sectional area, there is a corresponding increase in admittance and pressure.

Bauer et al[24] used an experimental setup consisting of three uniform tubes with diameters being inversely proportional to their impedances, and the waves were analysed in the frequency domain. The results only showed the alteration in the amplitude of pressure but yielded no information about the location of reflection or the origin of the backward wave. Also in an experimental study, Reuderink et al,[25] using the pressure measurement at three different points, "three-point method," studied the effect of tapering to validate the propagation coefficient. The authors used Womersley's theory to calculate the longitudinal and transversal impedance and compared the results with those obtained using the foot-to-foot method. They concluded that the increase in the tapering angle leads to higher discrepancies. In their study, they attempted to prove that the reflections are not generated by one isolated origin but a superimposition of multiple reflection sites, although re-reflected waves were not considered.

Segers and Verdonck[26] evaluated the tapered aorta as segments of a transmission line mathematical model. They concluded that the reflection present in the aorta is the outcome of two interacting phenomena: the continuous reflection caused by tapering and reflections originating from the diaphragm level. Using the frequency domain approach, the authors observed that the continuous reflection caused by tapering is hidden in the input impedance pattern.

More recently, Mynard and Smolich[27] computationally assessed the waves in diastole using a 1D-Wk mathematical model, and they compared changes of diameter in three different simulations: two stepwise and three stepwise diameter

reductions and a continuous tapered structure; their results showed that in the tapered tube, waves are merged and the pressure decays smoothly.

The 1D model has the ability to capture the distributed nature of the waves and their reflections in the arterial tree with a fair computational cost compared with 3D models. Moreover, unlike 0D models, it considers waves to be non-periodic.[28,29] 1D models have been used for explaining the phenomena happening in the arterial tree[30] and comparing it with in vivo[31-34] and in vitro[35-38] experiments.

To the best of our knowledge, most of the previous studies on the problem of tapering have applied the transmission line theory using frequency-based methods, and none investigated the effect of tapering on wave intensity analysis (WIA). Therefore, the aim of this work is to investigate the effect of vessel tapering on the changes of pressure and flow waveforms using a non-linear 1D time-domain model. We also aim to investigate the effect of varying the tapering angle on WIA.

2 | METHODS

We describe the governing mathematical equations and paradigms used for 1D modelling (Section 2.1) and WIA (Section 2.2). In Section 2.3, the studied 1D models, their properties, and input and output boundary conditions are presented.

2.1 | 1D formulation

The 1D, non-linear equations considered in this work assume blood to be an incompressible and Newtonian fluid flowing within an elastic, circular tube. The vessels' wall is assumed to be thin, homogeneous, and incompressible. The physical principles of conservation of mass and momentum[39] can be written as

$$\frac{\partial A}{\partial \mathrm{t}} + \frac{\partial (AU)}{\partial x} = 0, \tag{2}$$

$$\frac{\partial U}{\partial t} + U\frac{\partial U}{\partial x} = \frac{-1}{\rho}\frac{\partial P}{\partial x} + \frac{f}{\rho A}, \tag{3}$$

respectively, where x is the axial coordinate along the segments, t is the time, $U(x, t)$ is the mean blood axial velocity, A (x, t) is the cross-sectional area, and $P(x, t)$ is the internal pressure. The friction force per unit length is given by $f = -2(\gamma + 2)\mu\pi U$, where $\gamma = 9$ is determined by the prescribed shape of the velocity profile.[40] The pressure-area relationship (Equation 4) is required for closing the system of governing equations

$$P = P_0 + \frac{\beta}{A_0}\left(\sqrt{A} - \sqrt{A_0}\right). \tag{4}$$

A_0 is the area initial condition where $(P, U) = (P_0, 0)$, and β represents the material properties of the elastic vessel

$$\beta = \frac{4}{3}\sqrt{\pi}Eh, \tag{5}$$

where $E(x)$ is Young's modulus and $h(x)$ is the wall thickness. In this study, wave speed of the, also known as pulse wave velocity, $PWV(x)$, is calculated using the Moens-Korteweg equation

$$PWV_{MK} = \sqrt{\frac{\beta}{2\rho A_0}}\, A^{\frac{1}{4}}. \tag{6}$$

Equations for the conservation of mass and momentum (Equations 2 and 3) and pressure-area relationship (Equation 4) are solved using a discontinuous Galerkin numerical scheme with a spectral/hp spatial discretization.

Also, vessel junctions are calculated using the conservation of mass and continuity of total pressure.[15] A detailed explanation of the numerical modelling is provided in Alastruey et al.[41]

In addition to PWV_{MK}, which provides a local estimate for the pulse wave velocity in each cross-sectional area, a regional pulse wave velocity (PWV_{ff}) can be estimated by measuring the transient time and the path length between two different sites, using the foot-to-foot technique. $PWV_{ff}$is calculated as $\Delta L/\Delta t$, where ΔL is the axial difference between the measurement sites and Δt is the time it takes the waveform to travel from one measurement site to the other. In PWV_{ff}, the foot of the wave is considered as the intersection point of the end-diastolic decline and early-systolic rise sections of the pressure waveform.[42]

2.2 | Wave separation and WIA

Any disturbance in the flow creates a wave, propagating with speed $U + c$ in the forward direction and $U - c$ in the backward direction.[28] The forward pulse wave travels away from the heart to the periphery, and the backward pulse wave returns to the heart. Both pressure and velocity can be separated into their forward and backward travelling components. Total changes of velocity and pressure can be linearly separated into their corresponding forward (f) and backward (b) components, $dU = dU_f + dU_b$ and $dP = dP_f + dP_b$.[34,35,43,44] Combining these equations with the "water-hammer" formula, the change of pressure and velocity in the f and b directions can respectively be determined as previously shown[44-46]

$$dP_{f,b} = \frac{1}{2}(dP \pm \rho c dU),\ dU_{f,b} = \frac{1}{2}\left(dU \pm \frac{dP}{\rho c}\right). \tag{7}$$

The non-linear separation of waves has previously been presented in several studies.[47-59] However, Equation (7) is mostly used for practical applications through WIA.

Wave intensity (dI) is defined as the flux of energy carried by the wave per cross-sectional area[28] and can be calculated as $dI = dPdU$, having an SI unit of W/m^2. The intensities travelling into the f and b directions can be calculated as

$$dI_{f,b} = dP_{f,b}dU_{f,b} = \pm\frac{1}{4\rho c}(dP \pm \rho c dU)^2. \tag{8}$$

A forward travelling wave has a positive value ($dI > 0$), while the backward wave has a negative value ($dI < 0$). Waves can also be categorized based on their effect on pressure; a compression causes an increase but an expansion (decompression) causes a decrease in pressure.

In normal physiological condition, during early systole, a forward compression wave (FCW) increases both pressure and blood velocity.[50,51] During mid-systole, the arrival of a backward compression wave (BCW) causes an increase in pressure but a decrease in velocity. Then, in late systole, both pressure and blood velocity decrease as the result of the third wave forward expansion wave (FEW). Another FCW is expected during aortic valve closure due to a brief increase in pressure.[52]

2.3 | Simulations of 1D models

Five different sets of simulations (studies) are used to study the reflected waves in a tapered vessel. The first study revisits the traditional approach used in other studies,[21,23] which is a stepwise reduction of the area in a vessel, in time domain (Section 1). In the second study, we compare a straight vessel, a continuously tapered vessel, and a four and five stepwise reductions in diameter to highlight the difference between methods of modelling tapering (Section 2). A combination of the stepwise tapered vessel connected to a bifurcation is examined in three different lengths (Section 3). The fourth simulation is a model of the thoracic aorta, which is used for studying the effect of different tapering angles (Section 4). Then, a more complex model of the aorta consisting of the thoracic aorta connected to an iliac bifurcation is studied in Section 5.

2.3.1 | Reflections in three stepwise area reduction

In order to analyse the discrete reflections originating from a tapered structure, a vessel composed of three 5-m long segments with stepwise decreasing diameter was designed. The aim of this experiment is to trace the path of reflections and their time of occurrence in a simple setup, where the effect of tapering is magnified by using the stepwise reduction of the diameter.

A half-sinusoid flow wave is prescribed at the inlet of the structure, and changes in pressure are measured in the inlet of each segment. The decrease in diameter was uniform, and each succeeding segment has a diameter 10% smaller than the previous, in order to represent a crude effect of a tapered structure. The dimensions and properties are presented in Table 1. The 5-m long segments provide enough distance and travel time for reflections to emerge separately, since the calculated PWV_{MK} is 6.17 m/s. Figure 1A depicts the schematic representation of the structure.

2.3.2 | Reflections in stepwise diameter reduction and continuous tapered vessel

The three factors that describe tapering are the inlet diameter, the outlet diameter, and the length of the structure. A comparison between four and five stepwise reductions in the diameters of the vessel and continuously tapered vessel is made, as shown in Figure 1B. The inlet and outlet diameters of all structures are kept unchanged in the tapered structures. The tapering angle (θ) is calculated using

$$\tan\theta = \frac{D_{\text{in}} - D_{\text{out}}}{2L}, \tag{9}$$

TABLE 1 The dimensions and properties used in the structure with three stepwise reductions in diameter

Property	Description	Value (unit)
L_1, L_2, L_3	Length	5 (m)
A_{in1}	Diastolic area of segment 1	3.14 (cm^2)
A_{in2}	Diastolic area of segment 2	2.98 (cm^2)
A_{in3}	Diastolic area of segment 3	2.83 (cm^2)
h	Wall thickness	1.2 (mm)
E	Young's modulus	500 (kPa)
ρ	Blood density	1060 (kg/m^3)
μ	Blood viscosity	4 (mPa s)

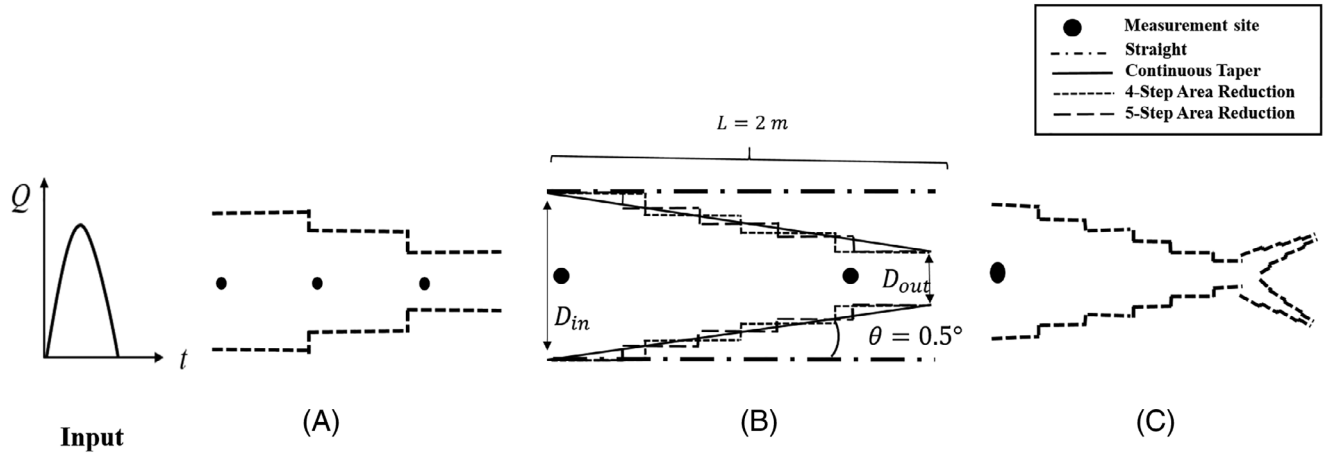

FIGURE 1 A schematic representation of (A) a tapered structure with three stepwise reductions in diameter, (B) stepwise tapering compared with a continuously tapered of a vessel, and (C) a combination of a stepwise tapering and bifurcation. The input for all experiments is a half-sinusoid flow waveform

where L is the length and D_{in} and D_{out} are the diameters at the inlet and outlet of all the vessels. The length of the vessel was assigned to be 2 m in order to highlight the overlapping of the reflected waves. The angle of tapering in this experiment is 0.5°, which falls into the range of physiological tapering.[26] The diameter at the inlet is 6 cm, which reduces to 2.5 cm at the outlet. The dimensions and properties used in the models are presented in Table 2. To avoid the reflections at the outlet, the terminal boundary condition is complete absorption.

2.3.3 | A combination of stepwise tapering and a bifurcation

A stepwise tapered bifurcation, as shown in Figure 1C, is simulated with three different lengths of segments to study the contribution of their reflections and the overlapping of waves as the segments become shorter. In the first case, the length of the mother vessel is 30 m in total, which consists of six segments that are 5 m. The daughter vessels are 5 m each, divided into five 1-m segments. In the next experiment, each segment is 16 times shorter than the previous structure, resulting in the mother tube and daughter tube to be 0.312 and 0.062 m, respectively.

Finally, in the third case, the length of the mother vessel is 0.469 m, with six 0.078 m segments, and the length of the branches are 0.390 m in total. The total length in the last case is reduced to 0.859 m, resembling the length of the aortic trunk and the iliac bifurcation. The blood viscosity and density in all experiments are 4 mPa s and 1050 kg/m^3, respectively. The inlet boundary condition is a half-sinusoid flow waveform. The duration of the flow is 0.5 second and the peak of flow is 20 L/min. As in the previous section, the outlets of the daughter vessels are completely absorbent. The length and diastolic area of segments are presented in Table 3.

2.3.4 | Tapering in the upper thoracic aorta

The model used for the upper thoracic aorta is a single vessel with constant wall thickness, connected to a three-element Wk model as the terminal boundary condition, and has been previously used in various studies.[44,53] The three

TABLE 2 The properties used in the comparison of four stepwise and five stepwise diameter reductions, continuous tapered, and straight vessel

Property	Description	Value (unit)
L	Length	2 (m)
A_{in}	Diastolic area of inlet	28 (cm^2)
A_{out}	Diastolic Area of outlet	4.94 (cm^2)
h	Wall thickness	1.2 (mm)
E	Young's modulus	500 (kPa)
ρ	Blood density	1060 (kg/m^3)
μ	Blood viscosity	4 (mPa s)

TABLE 3 The dimension of vessels used in tapered vessels and a bifurcation

	Experiment 1		Experiment 2		Experiment 3	
Property	Parent vessel	Daughter vessels	Parent vessel	Daughter vessels	Parent vessel	Daughter vessels
L, length (m)	30	15	1.87	0.94	0.55	0.27
A_d, diastolic area (cm^2)	3.14	1.18	3.14	1.18	3.14	1.18
h, wall thickness (mm)	1.20	1.20	1.20	1.20	1.20	1.20
E, Young's modulus (kPa)	400	400	400	400	400	400

Note: In Experiment 1, the segments are 5 m long; in Experiment 2, the length of each segment is 0.3125 m; and in Experiment 3, the segments are 0.07 m long.

TABLE 4 The properties used in the thoracic aorta model taken from Xiao et al[53]

Property	Description	Value (unit)
L	Length	24.1 (cm)
A_{in}	Diastolic area of inlet	4.5 (cm^2)
h	Wall thickness	1.2 (mm)
E	Young's modulus	400(kPa)
A (x,0)	Initial cross-sectional	3.06 (cm^2)
U (x,0)	Initial flow velocity	0
P (x,0)	Initial pressure	0
ρ	Blood density	1060 (kg/m^3)
μ	Blood viscosity	4 (mPa s)
R_1	Windkessel resistance	1.175×10^7 (Pa s m^{-3})
R_2	Windkessel resistance	1.116×10^8 (Pa s m^{-3})
C	Windkessel compliance	1.016×10^{-8}(m^3 Pa^{-1})

elements of Wk model are the proximal resistance, R_1, distal resistance, R_2, and a compliance, C. R_1 is connected in series with the parallel combination of R_2 and C.

Table 4 shows the values that are used in the model. The outlet cross-sectional area varies in relation to the tapering angle. The physiological tapering angle in human vessels has been reported to be up to 1.5°.[26] The inflow boundary condition was also described in Xiao et al.[53]

According to Epstein et al,[45] if the nonlinearities and the inertia terms are neglected, and it is assumed that pulse wave transit durations along a vessel is much smaller than the duration of the cardiac cycle, then the arterial compliance (C_v) and resistance (R_v) can be derived by

$$C_v = \frac{K_1}{\rho}, K_1 = \int_0^l \frac{A_0}{PWV_0^2} dx, \tag{10}$$

$$R_v = 2(\gamma + 2)\pi\mu K_2, K_2 = \int_0^l \frac{1}{A_0^2} dx. \tag{11}$$

2.3.5 | Tapering in the aorta and iliac bifurcation

A symmetrical iliac bifurcation is connected to the upper thoracic aorta with its side branches, namely, brachiocephalic, left carotid and left subclavian, and the descending thoracic aorta. The descending thoracic aorta is modelled as a straight vessel with constant wall thickness and no side branches. According to the finding of Hickson et al,[9] with ageing, the aortic arch increases both in length and cross-sectional area; therefore, in this study, we apply different tapering angles only on descending aorta. The linear tapering is implemented by changing the diameter at the end of the descending aorta using Equation (9). The area and the wall thickness of other segments are kept constant.

The terminal boundary condition for the iliac vessels is a three-element Wk model. The parameters used in the models are presented in Table 5 and in agreement with the findings of other studies.[10,46] The blood viscosity and density are 2.5 mPa s and 1040 kg/m^3, respectively. The initial pressure and velocity are defined as $(A_0, U_0) = (A_d, 0)$.

The inlet diameter was kept unchanged so that the interaction of the input boundary condition and the model remains the same. In addition, the area ratio of the aorta (the parent vessel) and the iliac vessels (the daughter vessels) are 0.97[16,57] in all simulations, which means that the iliac cross-sectional area is changed with the outlet area of the aorta to keep the ratio constant.

TABLE 5 Parameters used in the aorta and iliac bifurcation model

Segment number	Arterial segment	Length (cm)	R_{in} (mm)	R_{out} (mm)	Peripheral resistance (10^{10} Pa s m $^{-3}$)	Peripheral compliance (10^{-10} m ^{3} Pa^{-1})
1	Ascending aorta	6	17.80	17.80	—	—
2	Aortic arch I	2	15.30	15.30	—	—
3	Aortic arch II	3.9	6.60	6.60	—	—
4	Aortic arch III	5.2	7.86	7.86	—	—
5	Brachiocephalic	3.4	7.80	7.80	0.061	22.20
6	Left carotid	13.9	10.00	10.00	0.136	2.82
7	Left subclavian	3.4	9.53	9.53	0.139	12.16
8	Descending aorta II	24	12.60	12.60 → 8.44	—	—
9	Right common iliac	8.5	12	9.27 → 6.26	0.026	31.00
10	Left common iliac	8.5	12	9.27 → 6.26	0.026	31.00

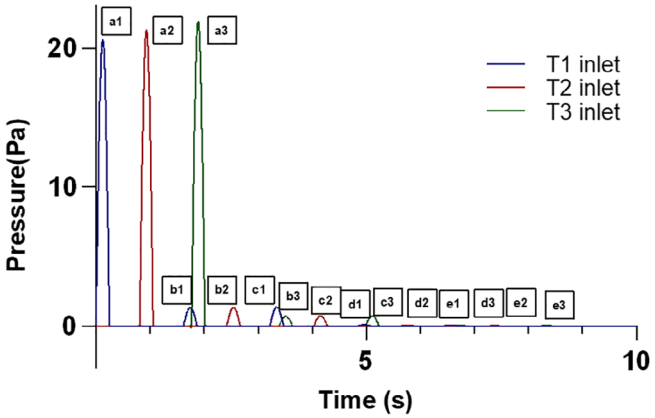

FIGURE 2 The pressure at the inlet of the first (blue), second (red), and third (green) segments in the three stepwise model

3 | RESULTS AND DISCUSSION

In this paper, we use simplified arterial haemodynamic models to highlight wave reflection patterns and their corresponding time of arrival. The tapering was first defined with a stepwise reduction of cross-sectional area, which was proposed in earlier studies.[23,24,27,58] The results of each model are discussed.

3.1 | Reflections in three-step area reduction

The pressure at the inlet of each segment is presented in Figure 2. The description of each pressure pulse is presented in Table 6. The negative sign behind the segment number stands for the reflection route.

As the pulse travels across each junction with decreasing cross-sectional area, the pressure increases (waves a1, a2, and a3). Further, a reflection travelling back to the inlet is generated at each junction (waves b1 and b2). After the first junction, the reflections are re-reflected (wave d1) and the amplitude of the wave reduces. In some cases, reflections overlap and emerge as one reflection (wave b2). Similar to the waves stated in Table 6, there are many reflections that appear on the pressure waveform; however, allocating their origin may not be straightforward since the system will include multireflection and re-reflected waves, some of which maybe an amalgamation of two or more re-reflections.

TABLE 6 Description of each pressure wave appearing in the experiment

		time	
Wave	**Path**	**Simulation**	**Theoretical**
a1	Input	0	0
a2	1	0.808	0.81
b1	1,−1	1.615	1.62
a3	1,2,3	1.762	1.767
b2	1,2,−2	2.405	2.409
c1	1,2,−2,−1	3.214	3.219
b3	1,2,−2,2,3	3.372	3.367
c2	1,2,−2,−1,1	4.026	4.029
d1	1,2,−2,2,−2,−1	4.835	4.819
c3	1,2,−2,−1,1,2,3	4.978	4.987
d2	1,2,−2,2,−2,−1,1	5.633	5.629
e1	1,2,−2,2,−2,2,−2,−1	6.438	6.418
d3	1,2,−2,2,−2,−1,1,2,3	6.614	6.581
e2	1,2,−2,2,−2,2,−2,−1,1	7.266	7.228
e3	1,2,−2,2,−2,2,−2,−1,1,2,3	8.204	8.186

These results, although obtained from a simplified model with non-physiological dimensions, show the difficulties of resolving the ongoing debate of localizing the origin of the reflections.

The PWV_{MK} of each segment was calculated at the inlet (seg1: 6.17 m/s, seg2: 6.25 m/s, seg3: 6.33 m/s) and compared with the PWV_{ff}, which is 6.25 m/s. For calculation of the arrival time of reflections, both local and foot-to-foot values were used. However, the local *PWV* better estimated the time of arrival of reflections, and the estimated time was closer to values produced from simulations.

Since the reflections that aroused from tapering are closely dependent on the local mechanical properties of the arterial wall, applying the foot-to-foot method is not convenient for locating their origin.

While in previous studies[23,25,27] the frequency domain was used for the analysis of the stepwise taper, using a time domain-based analysis gave us the ability of estimating the axial distance of the reflections as shown in Table 6. Figure 3 shows the calculation of the time and location of each reflection and the pattern of their generation.

3.2 | Reflections in stepwise diameter reduction and continuous tapered vessel

A systematic comparison between different methods of implementing tapering in 1D, such as continuous taper or stepwise reduction, and a straight segment was performed. The pressure waves at the inlet (A) and after 1.5 m (B) are shown in Figure 4. The inlet area and flow were kept constant in all simulations, which should generate the same input flow. However, the continuous tapered structure presents a higher peak pressure compared with other structures (Figure 4A).

The increase in input pressure is due to the increase of impedance in the first segment, which is in agreement with findings of Segers and Verdonck.[26] In addition, the continuous taper causes a smooth increase of reflections travelling to the inlet while the stepwise reductions cause sudden oscillations (Figure 4A). As the number of stepwise segments increases, the pressure fluctuation decreases and the amplitude is closer to the continuous taper. While the pressure amplitude in a straight vessel remains unchanged, there is a three-fold increase in pressure for the tapered structures.

In contrast to the inlet, the pressure at the outlet (Figure 4B) is higher when the tapering is defined as stepwise reduction. This shows how tapering can smoothen the pressure wave as the cross-sectional area is reduced. This result is in agreement with that found by Mynard and Smolich,[27] studying the effect of tapering on reflections and the smooth pressure decay in diastole.

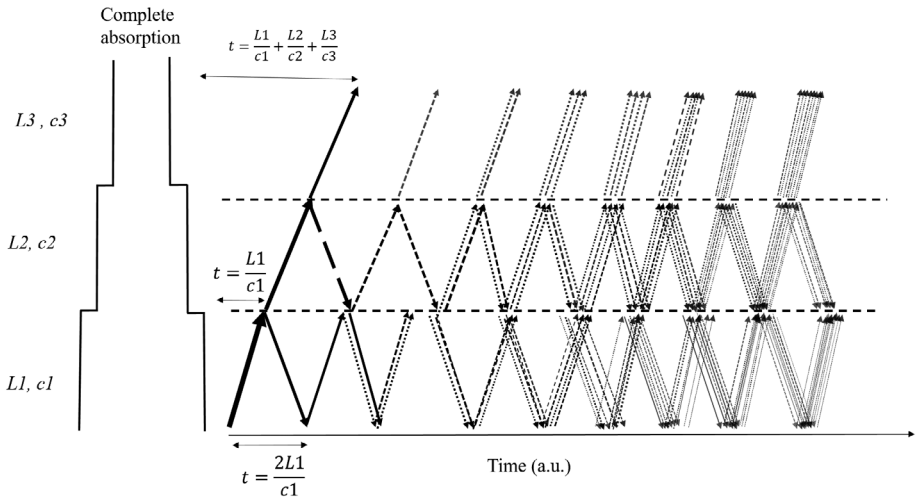

FIGURE 3 A schematic representation of stepwise tapering consisting of three segments and emerged reflections pattern. The lengths of all the segments L1, L2, and L3 are 5 m. c1, c2, and c3 denote for wave speed in the respective segments

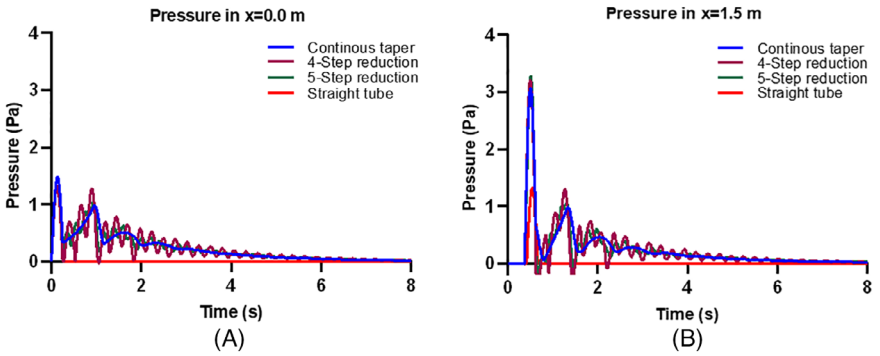

FIGURE 4 The pressure in the inlet (A) and the outlet (B) of a continuous tapered, five-step diameter reduction, four-step diameter reduction and a straight vessel

3.3 | A combination of stepwise structure and bifurcation

We performed a comparison between stepwise structures when the segments are 5 m in length and when the length of the segments are reduced to, first 0.312 m, and then 0.078 m. Figure 5 shows the computed pressure at the inlet of all the structures. Each junction, which is an imitation of the effect of tapering, causes a reflection wave to travel towards the inlet. A higher reflection is generated as the flow perturbation reaches the bifurcation, and the staggered arrangement of the daughter vessels creates a fluctuation in the reflections originated from the bifurcation.

All three models have the same inlet area; therefore, the flow should produce the same pressure amplitude at their inlets. However, Figure 5 shows a higher pressure in Experiment 3 compared with other simulations. This indicates that since the reflections do not have enough axial distance to emerge separately, they overlap each other and cause an increase in input impedance and, as a consequence, the pressure amplitude elevates. The reflections from the reduction of diameter are manifested as a constant pressure, while the reflection from the bifurcation causes a peak in pressure. The staggered definition of the daughter vessels caused a higher amplitude for the peak pressure, but the corresponding ripple effect, which is evident in Experiment 1, disappears in Experiment 3. The results of this study show the location and the time of occurrence of the reflections in long vessels. The length reduction adds complexity to the allocation of the origin of each reflection, which is also reported in other studies.[26,27] Therefore, we used WIA at the inlet of each structure to study the reflections and their occurrence time. (Figure 5, bottom).

Experiment 1 shows that only the reflections originating from the tapered bifurcation are detectable at the inlet. The same phenomenon is seen in Experiment 2; however, the occurrence time of reflection reaching to the inlet is decreased. Finally, Experiment 3 shows the amalgamation of the reflection, which is increasing the amplitude of backward wave intensity. It can be noticed that the FEW is decreasing when the reflection (BCW) is emerging, and it is not symmetrical with FCW.

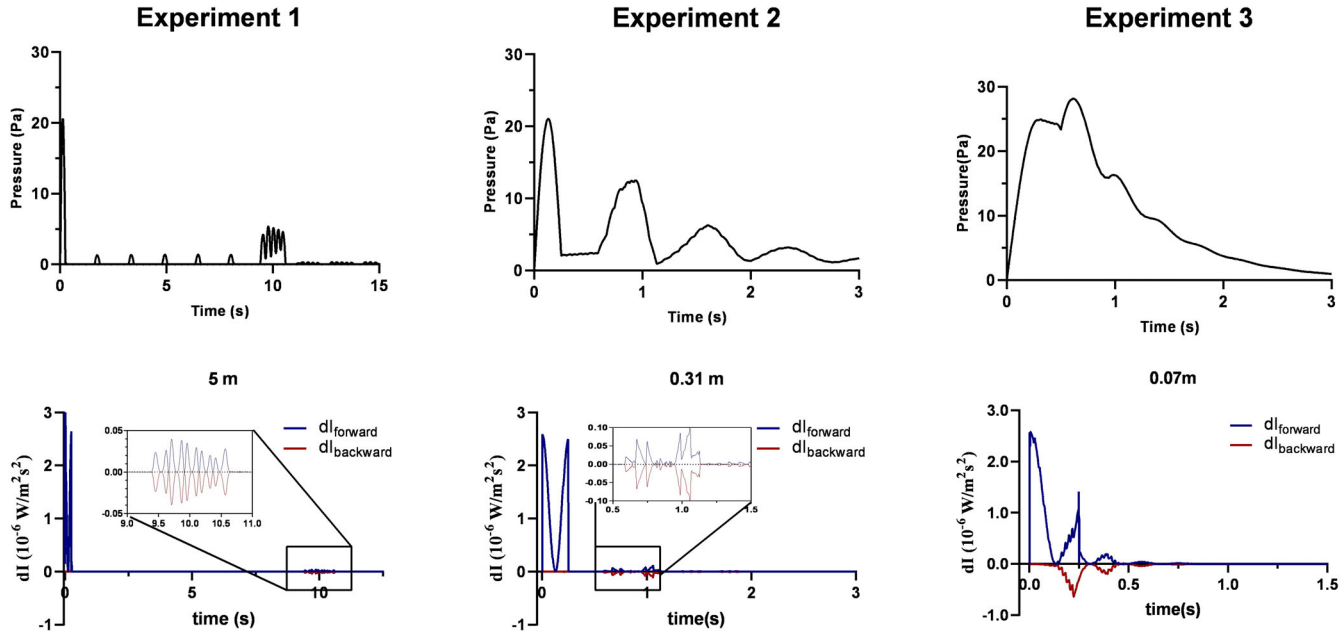

FIGURE 5 The pressure (top) and wave intensity analysis (bottom) at the inlet of a stepwise structure with segments 5 m long (Experiment 1), 0.312 m (Experiment 2), and 0.078 m (Experiment 3). All the structures have the same mechanical properties except the axial length of its consisting segments. The structure ends with a bifurcation, where the daughter tube diameter is reduced in the same manner

TABLE 7 Different tapering angles in thoracic aorta and the value pulse wave velocity in the inlet, outlet, mean, and the foot-to-foot method

Tapering angle θ (°)	PWV_{inlet} (m/s)	PWV_{outlet} (m/s)	PWV_{mean} (m/s)	PWV_{ff} (m/s)
1.375	5.016	6.974	5.995	6.352
1.250	5.016	6.696	5.856	6.351
1.125	5.016	6.448	5.732	6.034
0.875	5.016	6.026	5.520	6.032
0.750	5.016	5.844	5.429	5.746
0.625	5.016	5.677	5.346	5.485
0.375	5.016	5.382	5.199	5.247
0.00	5.016	5.015	5.015	5.028

Abbreviation: PWV, pulse wave velocity.

3.4 | Tapering in the upper thoracic aorta

With an increase in the tapering angle and a constant wall thickness, the PWV_{MK} increases in each cross-section. The difference in the $PWV_{ff}$is 1 m/s from no taper to the highest angle. The angles and the corresponding PWV_{MK}at the inlet and outlet, as well as mean and foot-to-foot *PWV*, are presented in Table 7. Several studies on age-related arterial stiffness reported an increase in *PWV* with age,[59,60] and a similar trend could be observed with the increase of tapering angle in the upper thoracic aorta model.

The pressure and the pulse pressure change have more evident differences as shown in Figure 6. The peak pressure at the inlet of the thoracic aorta changes by 5.72 kPa,from 0° to 0.87°.

The increase in mean pressure can be explained by the increase of arterial resistance in the thoracic aorta, which is in agreement with the results of.[2,6] In addition, a higher pulse pressure is reported in the ageing population, following the drop of diastolic pressure, which can also be seen in Figure 6.[2,61]

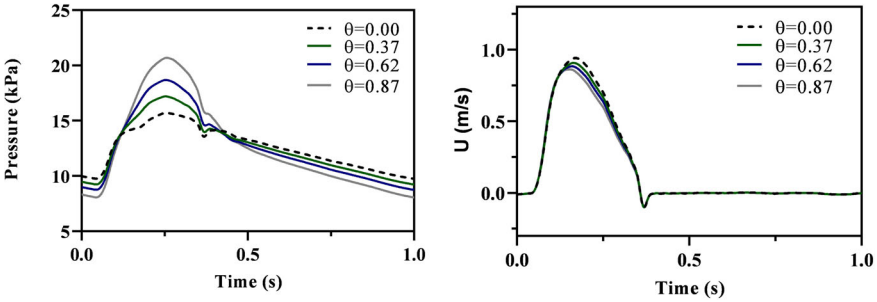

FIGURE 6 The measured pressure and flow velocity at the inlet of thoracic vessel in different angles of tapering

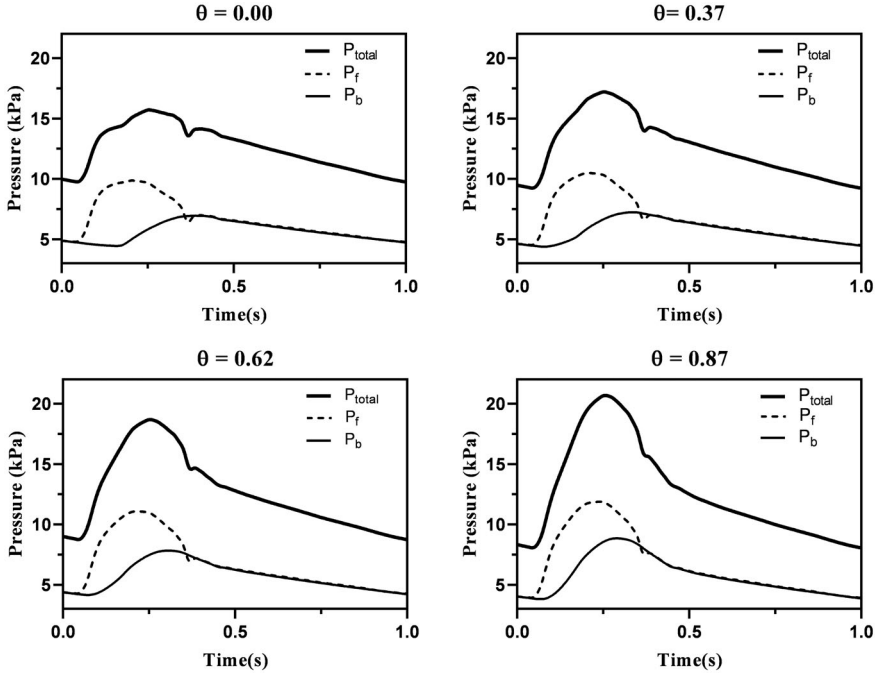

FIGURE 7 Forward and backward components of the pressure measured at the inlet of the upper thoracic aorta in different tapering angles

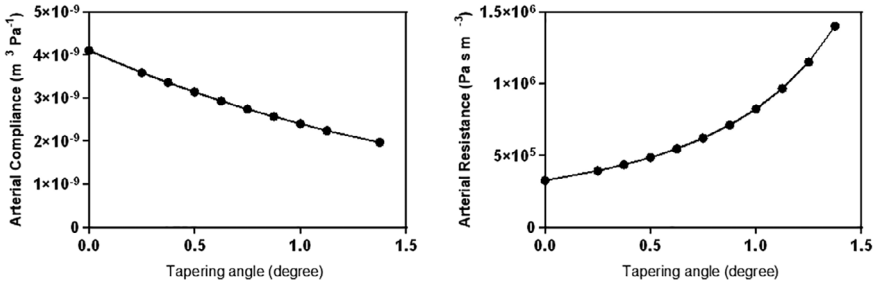

FIGURE 8 The arterial compliance (left) and resistance (right) changes with increased tapering angles

Furthermore, lower arterial compliance causes higher peak pressure in the aorta, since the damping ability of the arterial wall is lower.[7] Linear separation of the pressure at the inlet of the aorta with different angles is shown in Figure 7.

The arrival time of the backward travelling pressure (P_b) reduces as the difference in the inlet and outlet diameter increases, while the amplitude of both forward (P_f) and backward travelling pressure elevates.

The arterial compliance and resistance, computed using Equations (10) and (11), respectively, are presented in Figure 8. According to O'Rourke and Hashimoto,[62] the age-associated increase in systolic blood pressure is due to diminution of the arterial compliance. Our results show that with higher angle of tapering, arterial compliance decreases regardless of the value of Young's modulus. Consequently, the amplitude of systolic pressure rises with changes in diameters, which is in agreement with the results of clinical studies.[63]

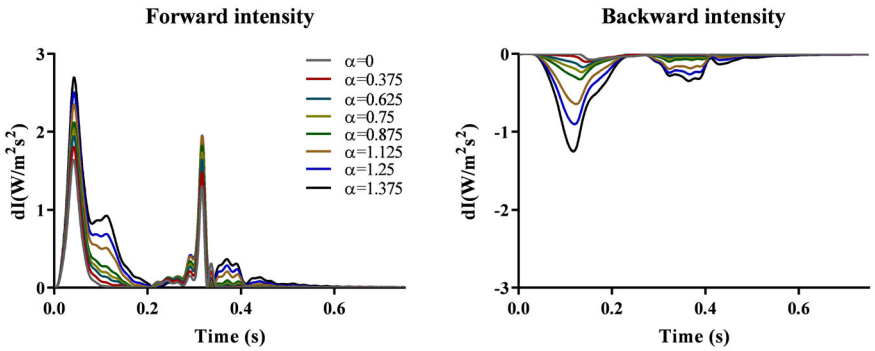

FIGURE 9 Wave intensity analysis at the inlet of the thoracic aorta with different tapering angles

Finally, we used WIA to study the reflections at the inlet of the thoracic aorta. A straight vessel causes a backward reflection due to the terminal resistance. As the cross-sectional area of the outlet becomes narrower, the amplitude of backward wave intensity increases. This surge is also evident in the forward wave intensity, which is anticipated because of the alteration in the arterial compliance and resistance.

While tapering causes an evident difference in the pressure at the inlet of the thoracic aorta, there is a negligible difference in the time of arrival of the backward waves (Figure 9).

The small variance of PWV_{ff} with tapering might explain the reason behind the time difference, which causes the reflection waves to arrive at the inlet at approximately the same time. In this model, we considered the wall thickness and Young's modulus to be constant throughout the vessel. The mentioned variables directly impact the PWV as they are included in Equation (6) (through Equation 5). However, according to O'Rourke et al,[64] the arterial wall becomes thinner towards the periphery.

3.5 | Tapering in the descending aorta and iliac bifurcation

The changes in diameter value had the same trend as the upper thoracic aorta model. Higher values of mean pressure, pulse pressure, and systolic pressure is observed with the increase of tapering angle.

The forward and backward components of the pressure measured at the inlet are shown in Figure 10. The increase in both forward and backward components of the pressure is noticeable in this model; however, the changes in the forward direction is lower compared with the backward component.

Figure 11 shows the wave intensity in the aorta when connected to the iliac bifurcation. FCW's amplitude has a small increase due to the constant properties of measurement location in all tapering angles. The BCW is growing in amplitude, and there is a gradual backward shift in time, which shows the early arrival of the reflections. The area ratio of the bifurcation is 0.97 in all the angles; therefore, the reflection caused by bifurcation is kept constant and the changes can be related solely to the effect of tapering. However, according to Greenwald et al,[16] the area ratio in iliac bifurcation decreases with ageing because the parent vessel's cross-sectional area expands while the cross-sectional area of the iliac vessel stays the same. In Mynard and Valen-Sendstad,[16] the pressure at the junctions are calculated, and they reported a higher accuracy of the simulations. Therefore, we suggest consideration of pressure losses at each junction to enhance the results.

Also, reflections originating from the side branches of descending aorta are neglected in this study, which can limit the accuracy of this model.

According to other studies,[2,9,61] pulse pressure and aortic impedance increase with stiffening of the vessel wall. In our simulations, we noted the same influence on pulse pressure and aortic impedance in increasing the angle of tapering. On the other hand, the changes in the arterial tree caused by ageing affect the proximal aorta more than its distal parts. In the ascending aorta, both the length and width increase, while in the descending aorta, only the diameter changes. This means that in the descending aorta, the angle of tapering increases with age.

We used the average values reported in Hickson et al[9] for length and diameter for different age groups. The result can be seen in Figure 12. Our findings are in agreement with the clinical values measured from 162 healthy subjects aged 18 to 77 years. In addition, our results provide a range of tapering angle for each decade of age group. We only used the values reported for the descending aorta.

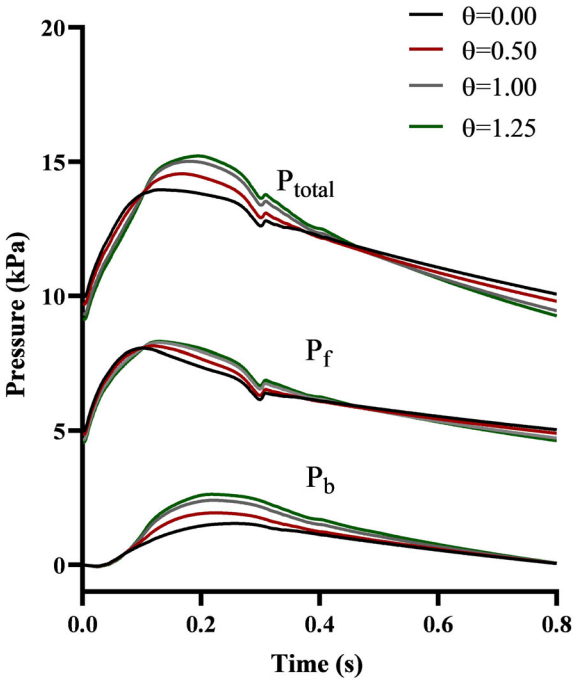

FIGURE 10 Pressure waveforms measured at the ascending aorta in the model of the aorta and iliac bifurcation. The pressure is separated into its forward and backward components in different tapering angles

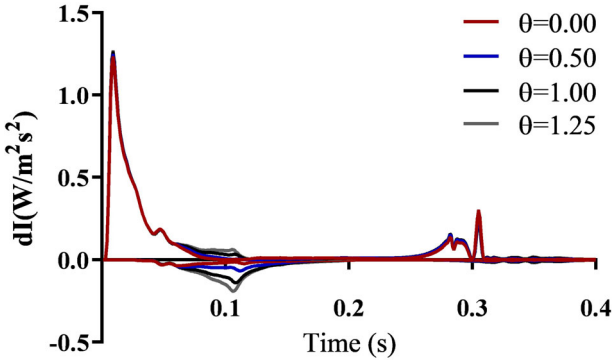

FIGURE 11 Wave intensity analysis at the ascending aorta. The model consists of the aorta connected to the iliac bifurcation. The tapering angle is changing in the descending aorta

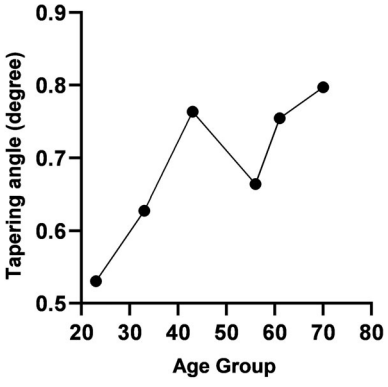

FIGURE 12 The reported variation of geometric tapering angle in descending aorta with ageing in Hickson et al. (2010)

The results show an increase in tapering angle in each age decade, except in 50-60. This appears to be an outlier due to the noise of the data.

It is known that ageing causes arterial wall thickness, elasticity, and changing of the wall layers.[7,62] It is reported that the elastic changes are smaller than geometrical changes in the arterial wall and can be neglected.[65] In all the

current simulations, we considered Young's modulus to be constant in each vessel and tapering angle. This consideration enabled us to focus on the alteration of diameter through aorta only. However, consideration of changes in elasticity can provide a better understanding of the ageing arterial wall.

In addition, the prescribed input boundary condition is constant even when the tapered vessel becomes narrower. This disregards the changes of the left ventricle with age and its response to changes in the proximal artery. Based on the findings of some studies,[6,60,66] left ventricle increases in mass and the walls changes (concentric remodelling); hence, changing the inflow boundary condition or the coupled model of the heart with each tapering angle can improve the results of this work.

Another limitation to this work is using the linear wave separation technique for examining the effect of tapering because tapering introduces additional non-linearity into the system and, as a consequence, assumptions on linearity can cause more substantial errors in the results, especially in steep tapered vessels.[47] Therefore, a non-linear analysis of the waves might provide a further understanding of the matter.

It is worth mentioning that the mathematical theories consider vessels as uniform circular tubes where the cross-sectional area and distensibility vary continuously. However, real blood vessels are of variable cross-sections and curved. Using the 1D model might be a crude heuristic method for the analysis of tapering since it neglects any flow movement in other directions. However, a comparison study between 1D and 3D models was conducted,[53] and the predictions of both simulations were in good agreement.

4 | CONCLUSION

We conclude that it is possible to show clear and discrete reflection sites in long segments (5 m). However, as the wave continues to travel, the reflection and re-reflection amalgamation cascades, limiting the ability to find the reflection sites. For segments with physiological lengths, the overlapping of the reflections causes an increase of pressure at the inlet of our computational models. Tapering not only causes a continuous reflection in the arterial structure but also increases the impedance of the system, which augments both peak and pulse pressures.

Additionally, the pressure variation throughout the segment is smoother in vessels with continuous tapered compared with stepwise changes in vessel area.

Increasing the tapering angle, as found in the ageing descending aorta, is associated with an increase in the peak pressure due to the increase of the segment resistance and an increase in pulse pressure due to the decrease in arterial compliance. Also, increasing the tapering angle caused an increase in the magnitude of both the forward and backward wave intensity.

Prospectively, a study of a larger number of arterial tree segments, compared with the current study that used different tapering angles, will provide more accurate information on the values of reflections with ageing. The effect of changes in Young's modulus, arterial wall thickness, non-linearity, and left ventricle concentric remodelling with tapering and ageing should also be included in future studies.

ORCID

Shima Abdullateef https://orcid.org/0000-0002-6091-7094

REFERENCES

1. Lakatta EG, Levy D. Arterial and cardiac aging: major shareholders in cardiovascular disease enterprises. *Circulation*. 2003;107(1):139-146.
2. O'Rourke MF, Nichols WW. Aortic diameter, aortic stiffness, and wave reflection increase with age and isolated systolic hypertension. *Hypertension*. 2005;45(4):652-658.
3. Learoyd BM, Taylor MG. Alterations with age in the viscoelastic properties of human arterial walls. *Circ Res*. 1966;18(3):278-292.
4. Redheuil A *et al*., Reduced ascending aorticstrain and distensibility earliest manifestations of vascular aging in humans. *Hypertension* 2010;55(2):319-326.
5. Sugawara J, Hayashi K, Yokoi T, Tanaka H. Age-associated elongation of the ascending aorta in adults. *JACC Cardiovasc Imaging*. 2008;1(6):739-748.
6. Redheuil A, et al. Age-related changes in aortic arch geometry: relationship with proximal aortic function and left ventricular mass and remodeling. *J Am Coll Cardiol.* 2011;58(12):1262-1270.
7. Collins JA, Munoz J-V, Patel TR, Loukas M, Tubbs ARS. The anatomy of the aging aorta. *Clin Anat.* 2014;27:463-466.
8. Caro CG, Pedley TJ, Schroter RC, Seed WA, Parker KH. *The Mechanics of the Circulation*. Cambridge: Cambridge University Press; 2011.

9. Hickson SS, Butlin M, Graves M, et al. The relationship of age with regional aortic stiffness and diameter. *JACC Cardiovasc Imaging*. 2010;3(12):1247-1255.
10. Charlton P, Harana JM, Vennin S, Li Y, Chowienczyk P, Alastruey J. Modeling arterial pulse waves in healthy aging: a database for in silico evaluation of hemodynamics and pulse wave indexes. *Am J Physiol Hear. Circ Physiol*. 2019;317:1062-1085.
11. Davies JE, Alastruey J, Francis DP, et al. Attenuation of wave reflection by wave entrapment creates a "horizon effect" in the human aorta. *Hypertension*. 2012;60(3):778-785.
12. Alastruey J, Parker KH, Peiró J, Sherwin SJ. Analysing the pattern of pulse waves in arterial networks: a time-domain study. *J Eng Math*. 2009;64(4):331-351.
13. Segers P, O'Rourke MF, Parker K, et al. Towards a consensus on the understanding and analysis of the pulse waveform: results from the 2016 workshop on arterial hemodynamics: past, present and future. *Artery Res*. 2017;18:75-80.
14. Stergiopulos N, Young DF, Rogge TR. Computer simulation of arterial flow with applications to arterial and aortic stenoses. *J Biomech*. 1992;25(12):1477-1488.
15. Olufsen MS. Structured tree outflow condition for blood flow in larger systemic arteries. *Am. J. Physiol. Circ. Physiol.* 1999;276(1):H257-H268.
16. Mynard JP, Valen-Sendstad K. A unified method for estimating pressure losses at vascular junctions, *Int. J. Numer. Method. Biomed. Eng.* 2015;31(7).
17. Khir AW, Parker KH. Measurements of wave speed and reflected waves in elastic tubes and bifurcations. *J Biomech*. 2002;35(6):775-783.
18. Abdullateef S, Mariscal-Harana J, Alastruey J, Khir A. "A Study on the Characteristics Influencing the Pressure at the Root of a Distributed One-Dimensional Model of Arterial Blood Flow," in 2018 Computing in *Cardiology Conference (CinC)*, 2019;45(1):4–7.
19. Greenwald SE, Carter AC, Berry CL. Effect of age on the in vitro reflection coefficient of the aortoiliac bifurcation in humans. *Circulation*. 1990;82(1):114-123.
20. Patel DJ, Freitas FMDE, Greenfield JC, Fry DL. Relationship of radius to pressure along the aorta in living dogs. *J Appl Physiol*. 1963;18: 1111-1117.
21. Lighthill MJ. Waves in fluids. *Commun. Pure Appl. Math*. 1967;20:267-293.
22. Pedley TJ. Mathematical modelling of arterial fluid dynamics. *Journal of Engineering Mathematics*; 2003;47:419-444.
23. Pedley TJ, Fung YC. The Fluid Mechanics of Large Blood Vessels. *J. Biomech. Eng*; 1980;102(4):345-346.
24. R. D. Bauer, T. Pasch, and E. Wetterer, "Theoretical studies on the human arterial pressure and flow pulse by means of a non-uniform tube model*+."
25. Reuderink P, Sipkema P, Westerhof N. Influence of geometric taper on the derivation of the true propagation coefficient using a three point method. *J Biomech*. 1988;21(2):141-153.
26. Segers P, Verdonck P. Role of tapering in aortic wave reflection: hydraulic and mathematical model study. *J Biomech*. 2000;33(3): 299-306.
27. Mynard JP, Smolich JJ. Wave potential and the one-dimensional windkessel as a wave-based paradigm of diastolic arterial hemodynamics. *Am J Physiol Circ Physiol*. 2014;307(3):H307-H318.
28. K. H. Parker, "An introduction to wave intensity analysis."
29. Willemet M, Alastruey J. Arterial pressure and flow wave analysis using time-domain 1-D hemodynamics. *Ann Biomed Eng*. 2014;43(1): 190-206.
30. Willemet M, Chowienczyk P, Alastruey J. A database of virtual healthy subjects to assess the accuracy of foot-to-foot pulse wave velocities for estimation of aortic stiffness. *Am J Physiol Heart Circ Physiol*. 2015;309(4):H663-H675.
31. Willemet M, Lacroix V, Marchandise E. Inlet boundary conditions for blood flow simulations in truncated arterial networks. *J Biomech*. 2011;44(5):897-903.
32. Steele BN, Wan J, Ku JP, Hughes TJR, Taylor CA. In vivo validation of a one-dimensional finite-element method for predicting blood flow in cardiovascular bypass grafts. *IEEE Trans Biomed Eng*. 2003;50(6):649-656.
33. Olufsen MS, Peskin CS, Kim WY, Pedersen EM, Nadim A, Larsen J. Numerical simulation and experimental validation of blood flow in arteries with structured-tree outflow conditions. *Ann Biomed Eng*. 2000;28:1281-1299.
34. Reymond P, Merenda F, Perren F, Rü D, Stergiopulos N. Validation of a one-dimensional model of the systemic arterial tree downloaded from. *Am J Physiol Hear Circ Physiol*. 2009;297:208-222.
35. Saito M, et al., One-Dimensional Model for Propagation of a Pressure Wave in a Model of the Human Arterial Network: Comparison of Theoretical and Experimental Results, 2011;133(12):121005(9 pages).
36. Zambanini A, Cunningham SL, Parker KH, Khir AW, McG.Thom SA, Hughes AD. Wave-energy patterns in carotid, brachial, and radial arteries: a noninvasive approach using wave-intensity analysis. *Am. J. Physiol. - Hear. Circ. Physiol.* 2005;289(1):H270-6.
37. Matthys KS, Alastruey J, Peiró J, et al. Pulse wave propagation in a model human arterial network: assessment of 1-D numerical simulations against in vitro measurements. *J Biomech*. 2007;40(15):3476-3486.
38. Bessems D, Giannopapa CG, Rutten MCM, Van De Vosse FN. Experimental validation of a time-domain-based wave propagation model of blood flow in viscoelastic vessels. *J Biomech*. 2008;41:284-291.
39. Peiró J, Veneziani A. Reduced models of the cardiovascular system. *Cardiovascular Mathematics*. Milano: Springer Milan; 2009:347-394.
40. Smith NP, Pullan AJ, Hunter PJ. An anatomically based model of transient coronary blood flow in the heart. *SIAM J. Appl. Math*. 2002; 62(3):990-1018.
41. J. Alastruey, K. H. Parker, and S. J. Sherwin, "Arterial pulse wave haemodynamics," *11th Int. Conf. Press. Surges*, no. October, pp. 401–443, 2012.

42. Gaddum NR, Alastruey J, Beerbaum P, Chowienczyk P, Schaeffter T. A technical assessment of pulse wave velocity algorithms applied to non-invasive arterial waveforms. *Ann Biomed Eng*. 2013;41(12):2617-2629.
43. Parker KH, Jones CJH. Forward and backward running waves in the arteries: analysis using the method of characteristics. *J. Biomech. Eng.* 1990;112(3):322.
44. Alastruey J, Khir AW, Matthys KS, et al. Pulse Wave Propagation in a Model Human Arterial Network: Assessment of 1-D Visco-Elastic Simulations against in vitro Measurements. *J Biomech*. 2011;44(12):2250-2258.
45. Laxminarayan S. The calculation of forward and backward waves in the arterial system. *Med. Biol. Eng. Comput.* 1979;17(1):130.
46. Westerhof N, Sipkema P, Bos GCVD, Elzinga G. Forward and backward waves in the arterial system. *Cardiovasc Res*. 1972;6(6):648-656.
47. Mynard JP, Davidson MR, Penny DJ, Smolich JJ. Non-linear separation of pressure, velocity and wave intensity into forward and backward components. *Med Biol Eng Comput*. 2012;50(6):641-648.
48. Pythoud F, Stergiopulos N, Meister JJ. Separation of arterial pressure waves into their forward and backward running components. *J. Biomech. Eng.* 1996;118(3):295.
49. Stergiopulos N, Tardy Y, Meister J-J. Nonlinear separation of forward and backward running waves in elastic conduits. *J Biomech*. 1993;26(2):201-209.
50. Khir AW, O'Brien A, Gibbs JSR, Parker KH. Determination of wave speed and wave separation in the arteries. *J Biomech*. 2001;34(9):1145-1155.
51. Kolyva C, Khir A. Wave intensity analysis in the great arteries – What has been learnt during the last 25 years? Part 1. *Int. Cardiovasc. Forum J*. 2015;1(2):68.
52. Kolyva C, Khir AW. Wave intensity analysis in the ventricles, carotid and coronary arteries—What has been learnt during the last 25 years?: Part 2. *Int Cardiovasc Forum J*. 2014;1(3):122-127.
53. Xiao N, Alastruey J, Alberto Figueroa C. A systematic comparison between 1-D and 3-D hemodynamics in compliant arterial models. *Int j Numer Method Biomed Eng*. 2014;30(2):204-231.
54. E. Boileau *et al*., "A benchmark study of numerical schemes for one-dimensional arterial blood flow modelling," *Int. j. numer. method. biomed. eng.*, vol. 31, no. 10, p. e02732, 2015.
55. Epstein S, Willemet M, Chowienczyk PJ, Alastruey J. Reducing the number of parameters in 1D arterial blood flow modeling: less is more for patient-specific simulations. *Am J Physiol Hear. Circ Physiol*. 2015;309:222-234.
56. Khir AW. What is it with patient's posture during intra aortic balloon pump therapy? *Artif Organs*. 2010;34(12):1077-1081.
57. Hardy-Stashin J, Meyer WW, Kauffman SL. Branching coefficient ('area ratio') of the human aortic bifurcation determined in distended specimens. *Atherosclerosis*. 1980;37(3):399-402.
58. Hall P. Unsteady viscous flow in a pipe of slowly varying cross-section. *J. Fluid Mech.* 1974;64(02):209.
59. Hallock P. Arterial elasticity in man in relation to age as evaluated by the pulse wave velocity method. *Arch Intern Med*. 1934;54(5):770-798.
60. Avolio AP, Chen SG, Wang RP, Zhang CL, Li MF, O'Rourke MF. Effects of aging on changing arterial compliance and left ventricular load in a northern Chinese urban community. *Circulation*. 1983;68(1):50-58.
61. Martin C, Sun W, Primiano C, McKay R, Elefteriades J. Age-dependent ascending aorta mechanics assessed through multiphase CT. *Ann. Biomed. Eng.* 2013;41(12):2565-2574.
62. O'Rourke MF, Hashimoto J. Mechanical factors in arterial aging: a clinical perspective. *J Am Coll Cardiol*. 2007;50(1):1-13.
63. Mitchell GF. Effects of central arterial aging on the structure and function of the peripheral vasculature: implications for end-organ damage. *J Appl Physiol*. 2008;105(5):1652-1660.
64. O'Rourke M, Farnsworth A, O'Rourke J. Aortic dimensions and stiffness in normal adults. *JACC Cardiovasc Imaging*. 2008;1(6):749-751.
65. Wemple RR, Mockros LF. Pressure and flow in the systemic arterial system. *J Biomech*. 1972;5(6):629-641.
66. Kim HL, Lim WH, Seo JB, Chung WY, Kim MA, Zo JH. Association between arterial stiffness and left ventricular diastolic function in relation to gender and age. *Medicine (Baltimore)*. 2017;96(1):e5783(6 pages).

How to cite this article: Abdullateef S, Mariscal-Harana J, Khir AW. Impact of tapering of arterial vessels on blood pressure, pulse wave velocity, and wave intensity analysis using one-dimensional computational model. *Int J Numer Meth Biomed Engng*. 2020;e3312. https://doi.org/10.1002/cnm.3312